Indian Journal of Biochemistry & Biophysics
Vol. 63, November 2026, pp. 1313-1326
DOI: 10.56042/ijbb.v63i11.21576

Understanding the effects of salinity and temperature variations on conformational changes in a thermohalostable lipase: Insights from molecular dynamics simulations

Risa Chintia Balqis[1], Febriani[1], Setyanto Tri Wahyudi[2] & Teuku Mohamad Iqbalsyah[1]*

[1]Biomolecules Application Research Group, Chemistry Department, Faculty of Mathematics and Natural Sciences, Universitas Syiah Kuala, Banda Aceh-23111, Indonesia

[2]Department of Physics, IPB University, Bogor-16680, Indonesia

Received 14 July 2025; *revised 28 October 2026*

The interplay between side-chain hydrogen bonds and salt bridge networks stabilises thermohalostable enzymes. This study examined the effects of NaCl (0.6, 2.0, and 4.0 M) and temperature (300, 343, and 373 K) on the conformation of thermohalostable lipase using molecular dynamics simulations. The simulation was done using the AMBER with the ff14sb force field for 100 ns in the TIP3P solvent. The enzyme showed minimal structural changes across various temperatures and NaCl concentrations, as indicated by slight variations in the root mean square deviation (RMSD), radius of gyration (Rg), and solvent-accessible surface area (SASA). While increasing temperature raised root mean square fluctuation (RMSF) values, NaCl concentration effects were only significant at 373 K. Minimal changes in the secondary structure composition support the suggestion of overall structural stability. The catalytic site remained stable, with slight differences in the RMSF values for the catalytic triad and oxyanion hole residues, although their orientation was altered. Higher temperatures decreased the number of hydrogen bonds, but salt ions compensated for this loss by enhancing electrostatic interactions with charged residues, which incurred energy costs. The 0.6 M NaCl concentration was optimal for lipase stability across the tested conditions. These results advance our understanding of the structural stability mechanisms in thermohalostable enzymes and may be used in the development of novel enzymes for industrial applications.

Keywords: Conformational change, Electrostatic interaction, Halostable, Hydrogen bond, Lipase, Salt effect, Temperature effect, Thermostable

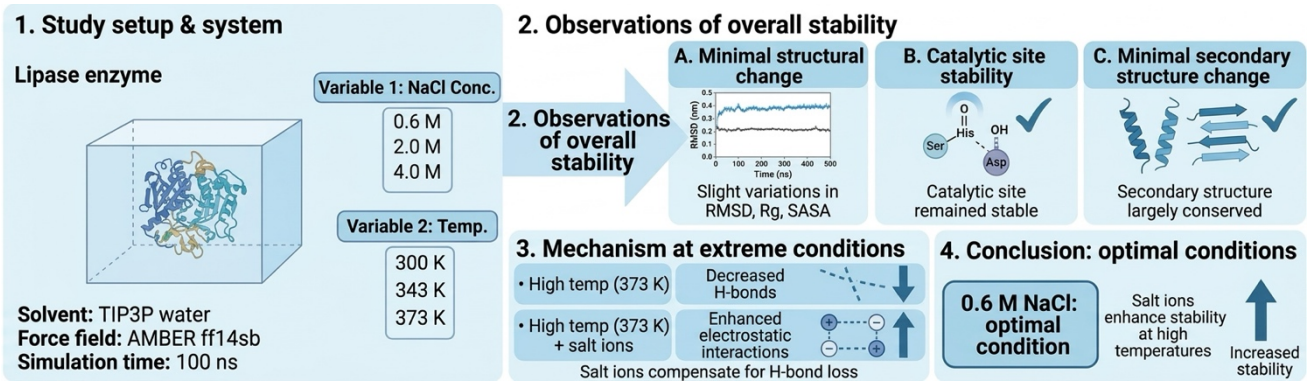
Extremophiles are microorganisms that thrive in harsh environments and exhibit unique biochemical and physiological adaptations. These habitats may have extreme temperatures, non-physiological pH levels, or increased salinity[1]. Extremophiles' adaptations are enabled by unique membrane composition, habitat-specific gene expression regulation, and specialised DNA repair mechanisms[2]. Their enzymes, known as extremozymes, are specifically adapted to function optimally under severe conditions[3]. Extensive research has been conducted on extremozymes to understand their stabilising mechanisms and utilise their potential for various applications[4,5].

A bacterial strain, designated PLS 80, was isolated from undersea fumaroles in the Pria Laot Sabang area of Aceh Province, Indonesia. As it thrives in high-temperature and high-salinity environments, it produces a 50-kDa lipase (triacylglycerol hydrolases - EC 3.1.1.3) that exhibits thermostability and halostability[6]. This enzyme catalyses the hydrolysis and transesterification of lipids at an optimal temperature of 70°C and pH 7. The three-dimensional structure of lipase has been predicted using homology modelling. Its conformational stability at various temperatures has been investigated computationally[7].

Thermo-halotolerant lipases have applications in the detergent, food, textile, cosmetic, paper, and pharmaceutical industries[8]. They act as efficient biocatalysts in industrial processes with high temperature and salinity, such as producing fermented foods and salt-preserved products[9]. Their stability has led to increased use in the pharmaceutical industry, where reactions in organic solvents are required [10]. They can also be used for bioremediation in lipid-rich saline environments[11].

Protein thermostability is primarily achieved through increased frequency of side chain hydrogen bonds[12,13] and salt bridges networks[14]. Stabilising salt bridges in thermostable enzymes are formed by polar

*Correspondence:
E-mail: t.iqbalsyah@usk.ac.id
Suppl. data available on respective page of NOPR



Graphical abstract

residues through short bond lengths and wide donor-hydrogen-acceptor (DHA) angles[15]. Therefore, charged and polar residues, particularly Arg and Glu[16,17], are present at a higher frequency than in mesophilic proteins. Other factors also support thermostability, although to a lesser extent, including distinct secondary structural elements[18], increased metal ion-binding sites, extended network aromatic-aromatic interactions[19], and the presence of disulfide bonds[20,21]. The positioning of proline in β-turns is also reported to increase stability by alleviating rigidity[22].

Protein halostability is predominantly achieved through salt bridge formation. Halophilic enzymes have distinct amino acid profiles with greater hydrophilicity and acidity[23]. Their structures are characterised by a higher occurrence of acidic residues on their surfaces than on their interiors. Unlike thermostable proteins, which maintain a balance between acidic and basic residues, they compensate for their negatively charged residues on the protein surface by having fewer basic residues[24,25]. Carboxyl groups in acidic residues on the surface help hydration and ion binding, promoting structural stability under saline conditions [26]. Furthermore, they exhibit a more flexible structure that facilitates effective interaction with water molecules to counteract the dehydration effects due to high salt concentrations[27]. The modified hydrophobicity also enhances their solubility in low water activity conditions[28], which arises from the distinct frequency of some amino acids[29].

Although charged residues play a significant role in both protein thermostability and halostability, their precise balance for optimising structural stability remains unclear. Halostable proteins exhibit increased flexibility, in contrast to the rigidity commonly associated with thermostable proteins. Therefore, understanding the equilibrium of side-chain hydrogen bonds and salt bridge networks in contributing to structural stability is crucial in a thermohalostable protein.

This study evaluated the simultaneous effects of temperature and salt concentration on the structure of lipase PLS 80 using Molecular Dynamics (MD) simulations with Assisted Model Building with Energy Refinement (AMBER)[30]. This study is an extension of our previous study that focused solely on the effect of temperature changes in a salt-free environment, which revealed that hydrogen bonding is significantly perturbed only at very high temperatures, increasing the molecular flexibility of some rigid residues[7]. As haloenzymes are generally polyextremophilic[31] and their stability is modulated by salt[32], it is important to evaluate the effect of salt concentration at high temperatures to better understand the role of salt bridges on the surface of thermohalophilic proteins. Conformational stability and dynamic structural changes were evaluated to predict the activity based on changes in the lipase catalytic region. The results of this study may provide better insights into how shared structural features affect the stability. Understanding the structural characteristics of thermohalostable enzymes could facilitate advancements in protein engineering.

Material and Methods

Lipase structure

The simulation used the 3D structure of lipase PLS 80, which consists of 383 residues. This molecule is a gene-translated structure that has been previously validated[7] (Fig. 1, and Suppl. Table 1).

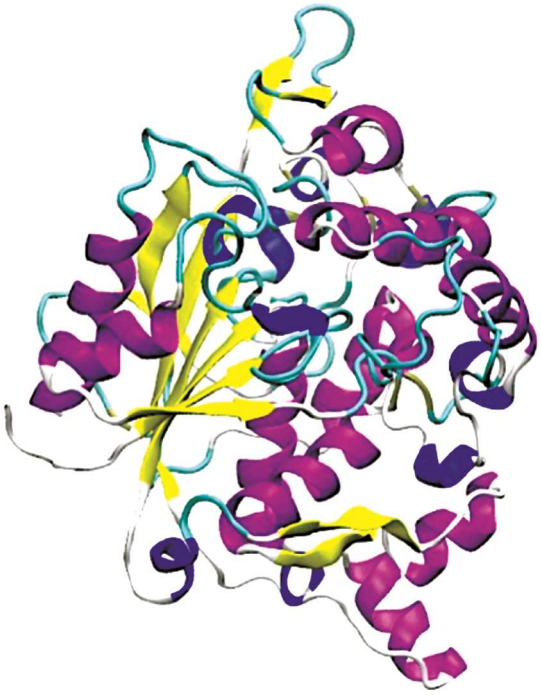


Fig. 1 — The 3D structure of lipase PLS 80, consisting of 383 residues, was used in the molecular dynamics simulation

Preparation of structure and topology

The lipase structure and topology were prepared by removing hydrogen atoms and identifying any missing atoms or gaps in the enzyme. pdb file. A topology file was created using pdb4amber in the Assisted Model Building with Energy Refinement (AMBER) version 22[33] using the ff14sb force field[34]. The protonation of specific residues was verified at http://biophysics.cs.vt.edu. The structure coordinates were aligned to the origin structure using the VMD software[35]. The PDB structure and system solvation parameters were incorporated using LEaP in AMBER. The solvent was a simple water model-type tip3p in a truncated octahedral box with a total volume of 587275.607 $Å^3$.

For the NaCl concentration variation simulation, the solvent system was supplemented with Na^+ and Cl^- ions, consisting of 166 Na^+ and 167 Cl^- for 0.6 M NaCl, 554 Na^+ and 555 Cl^- for 2 M NaCl, and 1107 Na^+ and 1108 Cl^- for 4 M NaCl. The amount of NaCl added was calculated using the SPLIT method in AMBER. Each treatment was performed at 300, 343, and 373 K.

The simulation was performed using the Periodic Boundary Condition (PBC) method in AMBER to eliminate surface tension effects and achieve uniform density and pressure. The SHAKE algorithm with a 10^{-5} tolerance was applied to constrain all the bonds involving hydrogen atoms. The system's electrostatic energy was calculated using the Particle Mesh Ewald (PME) method.

Preparation of the simulation system

The simulation system consisted of three steps: minimisation, heating, and equilibration. First, minimisation was performed by reducing bad contacts and high-energy steric effects in the solvated lipase molecule. Each simulation began with a 40-ps minimisation process to bring the structure to its lowest energy state using the SANDER feature in AMBER. The minimisation initially constrained all atoms, followed by non-hydrogen atoms. The constraints were then applied to the backbone atoms (C, O, and N), followed by the C_α atoms. Constraints on the C_α atom were applied using a Langevin Dynamics Thermostat[36]. Finally, all the constraints were released. The minimisation produced a restart file (*.rst) and an output file (*.mdout).

Secondly, the structure was heated with minimal energy using the .mdout file as the input. Initially, the system was set to 0 K and gradually heated to 300, 343, and 373 K using the NVT ensemble (constant number, volume, and temperature) for 1 ns. The system was coupled to a thermostat with velocity rescaling at a coupling constant of 0.1.

Finally, equilibration was performed to stabilise the system and mitigate thermodynamic disturbances. The inputs for this step were derived from the heating step. Initially, equilibration was performed using an NVT ensemble for 50 ps, followed by an NPT ensemble (constant number, pressure, and temperature) for 500 ps. The constraints from the heating step were then removed from the models. The system was equilibrated to achieve the target density, and Gamma_ln was added to represent the theoretical state of the solution. The equilibration process was continued for an additional 0.5 ns.

Production simulation

When the structure was well equilibrated, it was placed in the production run stage. The production was conducted in the NPT ensemble to control the pressure and temperature of the system. The constraints applied during the heating step were removed, allowing the molecules to move freely during equilibration. The production was carried out at temperatures of 300, 343, and 373 K for 100 ns for all NaCl concentrations. The output of the production simulation consisted of the coordinates and trajectory files of the structure, which were then analysed.

Table 1 — Differences in average RMSD, Rg, and SASA values at various temperatures and NaCl concentrations compared to the reference structure (343 K, 0.6 M NaCl).

Temperature (K)	[NaCl] (M)	The difference in the average value				
		RMSD (Å)	R_g (Å)	Total SASA (Å^2)	Polar SASA (Å^2)	Nonpolar SASA (Å^2)
300	0	-0.21	-0.19	-465	-279	-186
	0.6	-0.34	-0.18	-283	-134	-149
	2.0	-0.24	-0.20	-419	-259	-160
	4.0	-0.24	-0.22	-403	-190	-213
343	0	-0.03	-0.03	-43	-34	-10
	0.6	0	0	0	0	0
	2.0	-0.09	-0.17	-316	-207	-110
	4.0	-0.16	-0.14	-288	-193	-96
373	0	0.28	0.13	406	161	245
	0.6	0.13	-0.03	136	-54	189
	2.0	0.39	0.11	459	207	252
	4.0	0.07	-0.03	-51	-57	5

Analysis of simulation results

The simulation results were analysed using the features available in AmberTools. The parameters included Root Mean Square Deviation (RMSD), radius of gyration (R_g), solvent-accessible surface area (SASA), Root Mean Square Fluctuation (RMSF), total energy, hydrogen bonds, electrostatic interactions, secondary structure composition, and catalytic site area. Each parameter was analysed and evaluated by running commands on AmberTools22[30].

The RMSD was calculated using Equation 1 and plotted against the simulation time[37,38].

$$RMSD = \sqrt{\frac{\sum_{i=1}^{N}\left(r_i - r_i^{ref}\right)^2}{N}} \quad \ldots (1)$$

where N is the total number of Cα atoms, is the coordinates of the protein atoms, and is the coordinates of the reference atoms[38].

The RMSF provided information on the fluctuation of each residue during the simulation compared to the initial residue in the structure, which was calculated using Equation 2.

$$RMSF = \sqrt{\frac{1}{T}\sum_{t=1}^{T}(r_t^a - \overline{r^a})^2} \quad ,,, (2)$$

where T is the total number of time steps, r_t^a is the position of atom or residue a at time, and r^a is the average position of the residue[39].

The R_g value was calculated as a function of the atomic position relative to the centre of the protein mass[40]. The total energy was calculated as the sum of the energies of the bonds, dihedrals, angular and van der Waals interactions, and electrostatic interactions within the protein[41]. SASA analysis evaluates the surface area of a protein that is accessible to both polar and nonpolar solvents[42]. Secondary structure analysis measures compositional changes in the α-helix, β-sheet, 3_{10}-helix, coil, and turn structures[43]. Electrostatic interactions were calculated as the average number of salt bridges formed during the simulation. The interactions of Glu, Asp, Lys, and Arg, which can interact with Na^+ and Cl^- ions, were analysed[44]. The catalytic area was calculated based on the triangles formed by the catalytic triad comprising Ser110-Asp314-His355[7], using Heron's formula[45]. The calculation considered the dynamic nature of the triangle and was calculated using the centre of mass of the atoms in each triad residue. Structural analysis was performed to visually evaluate the changes in lipase conformation using VMD software[35].

Results

The change in lipase overall conformation

The conformational changes of lipase PLS 80 were studied at various temperatures (300, 343, and 373 K) and NaCl concentrations (0.6, 2.0, and 4.0 M) using the lipase structure at 343 K and 0.6 M NaCl as a reference structure. Table 1 shows the average values of the RMSD, R_g, and SASA during the 100 ns simulation. RMSD quantifies the structural deviation from the original conformation, whereas R_g indicates the structural compactness[37]. SASA quantifies the protein surface area accessible to solvents. Increases in RMSD, R_g, and SASA indicate structural expansion[42]. The RMSD, R_g, and total SASA of the reference structure were 1.29 Å, 20.19 Å, and 16,533 Å² (polar SASA of 11,837 Å² and nonpolar SASA of 4,696 Å²), respectively.

Table 1 presents the differences in the average RMSD, R_g, and SASA at various temperatures and

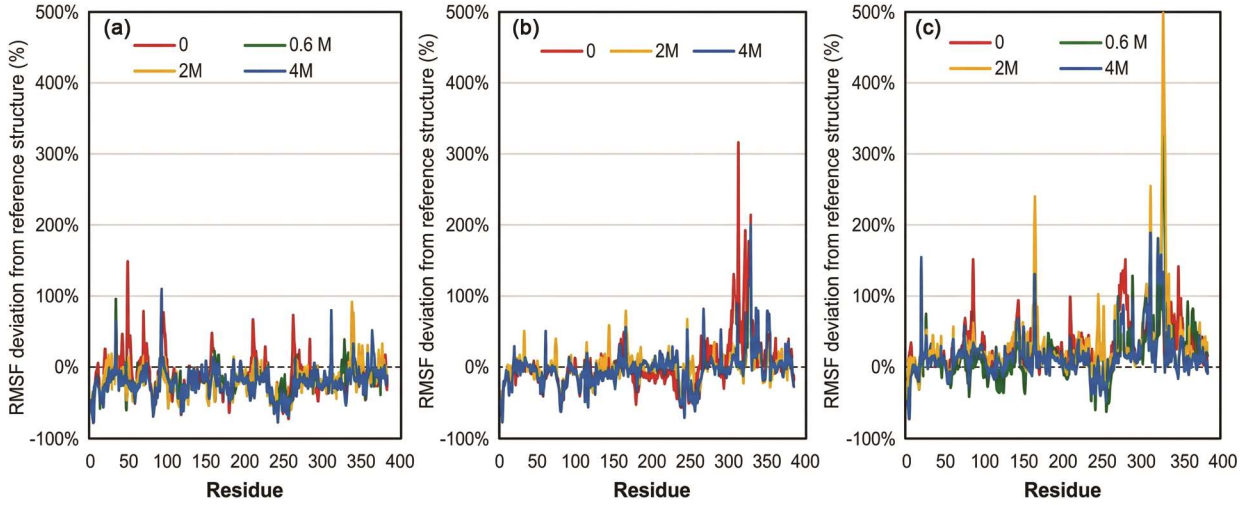


Fig. 2 — Percentage of RMSF deviation from the corresponding residues in the initial structure at various temperatures and NaCl concentrations. (a) 300 K, (b) 343 K, and (c) 373 K. (—) = 0, (—) = 0,6 M NaCl, (—) = 2 M NaCl, and (—) = 4 M NaCl

NaCl concentrations, relative to the reference structure. Negative values indicate lower measurements than the reference values, whereas positive values indicate the opposite. At 300 K, both RMSD and R_g were lower than those observed in the reference structure across all NaCl concentrations. At 343 K, the differences in RMSD and R_g were also negative, with more pronounced effects at 2 M and 4 M NaCl. At 373 K, the RMSD differences were positive for all NaCl concentrations, notably for 2 M NaCl. However, the R_g values varied, with slight structural compactness observed at 0.6 M and 4 M NaCl.

The values of the total, polar, and nonpolar SASA at 300 K were lower than those of the reference. The most significant reduction in total SASA was observed in the absence of NaCl. At 343 K, all SASA values remained below the reference, although they were less pronounced than at 300 K. At 373 K, the SASA exhibited unpredictable changes with increasing NaCl concentrations. A notable exception occurred at 4.0 M NaCl, where the structure showed reduced SASA.

The change in RMSF

While RMSD, R_g, and SASA provide insights into the overall lipase structure, RMSF identifies the extent of fluctuation of individual residues[37]. Low RMSF values indicate rigidity, whereas high values indicate increased flexibility[46]. Generally, the RMSF values increased with increasing temperature but varied randomly at different concentrations of NaCl. At 300 K, the RMSF values were generally low for all NaCl concentrations. As the temperature increased, regions 300-360 exhibited increased fluctuations. At 343 K, the residues without NaCl and those with 4 M NaCl showed greater flexibility. At 373 K, the residues in 2 M and 4 M NaCl displayed significant fluctuations of high magnitude within these regions (Fig. 2).

To determine whether this phenomenon occurs universally or is restricted to specific groups, the residues were analysed in clusters. A pattern was observed; the average RMSF values were consistently the lowest at 343 K. However, this was not the case when the RMSF was evaluated for all residues. The RMSF at 300 K was lower than that at 373 K under all simulation conditions. An analysis of variance (ANOVA) indicated that, at a 95% significance level, varying NaCl concentrations resulted in differences at each temperature only for all residues, nonpolar, and polar clusters at 373 K (Table 2).

The change in secondary structure composition

The fluctuation of residues due to various temperatures and NaCl concentrations may alter the secondary structure conformation; thus, the changes in the structural composition were compared with the reference. The reference structure comprised 28.7% α-helices, 15.8% β-sheets, 5.9% 3_{10}-helices, 19.4% coils, and 30.3% turns. Across all simulation parameters, the compositional differences were generally minor, ranging from -2.82% (turn at 343 K and 4 M NaCl) to 3.03% (α-helix at 343 K without NaCl). The α-helix composition changed variably, whereas β-sheet and 3_{10}-helix exhibited a general

decreasing trend with increasing temperature, albeit at varying degrees. The turn structure increased irregularly when the temperature and NaCl concentration increased. In addition, the coil demonstrated variability with increasing temperature or NaCl concentration (Table 3). The changes in α-helix were strongly correlated with changes in the sum of the 3_{10}-helix and turn conformations ($R^2 = 0.9241$).

As previously discussed, the RMSF in the 300-360 regions showed high fluctuation when the temperature increased. This region was further examined to assess alterations in the secondary structure. Generally, the β-sheet remained unaffected. However, a short 3_{10}-helix located in the middle of the reference structure showed conformational changes under various environmental conditions. This secondary structure either altered its orientation and length or transitioned to an α-helix.

Additionally, the secondary structure in the N-terminal region also underwent modification. It initially adopted a turn conformation in the reference structure but transitioned to a 3_{10}-helix at several environmental conditions. Nevertheless, no consistent pattern of changes was observed in relation to temperature or salt concentration (Fig. 3).

The change in the catalytic area

Overall conformational changes may also alter the lipase catalytic sites. Lipase PLS 80 contains a catalytic triad composed of Ser110-Asp314-His355[7]. The reference structure at 343 K and 0.6 M NaCl had an area of 23.82 Å². At 300 K, the catalytic area was generally smaller than the reference value, except at 0.6 M NaCl. At 343 K, the absence of NaCl led to a notable increase of 4.11 Å². At 2.0 M and 4.0 M NaCl, the area decreased by 2.78 Å² and 2.49 Å², respectively. At 373 K, the catalytic area increased with higher NaCl concentrations, except at 0.6 M NaCl, which showed a decrease of 1.19 Å². Although the changes in the catalytic area were minor, the orientation of the side chains was altered, potentially affecting catalytic efficiency (Fig. 4).

In addition to the catalytic triad, lipase activity is influenced by the oxyanion hole. In lipase PLS 80, the oxyanion hole is located at residues 7-12, consisting of Ile-Val-Leu-Leu-His-Gly[47]. This structural feature plays a crucial role in stabilising the negatively

Table 2 — Average RMSF values at various temperatures and NaCl concentrations

Cluster	Temperature	Average RMSF (Å)				ANOVA
		0	0.6 M NaCl	2 M NaCl	4 M NaCl	p-value
All residues	300 K	0.82 ± 0.35	0.77 ± 0.34	0.79 ± 0.37	0.79 ± 0.36	0.209
	343 K	1.01 ± 0.49	1.02 ± 0.50*	0.98 ± 0.40	0.94 ± 0.40	0.093
	373 K	1.26 ± 0.59	1.14 ± 0.54	1.30 ± 0.72	1.12 ± 0.49	0.00002**
Nonpolar	300 K	0.90 ± 0.41	0.93 ± 0.44	0.89 ± 0.31	0.85 ± 0.32	0.204
	343 K	0.75 ± 0.26	0.68 ± 0.23*	0.71 ± 0.29	0.71 ± 0.25	0.363
	373 K	1.14 ± 0.56	1.04 ± 0.45	1.15 ± 0.59	1.01 ± 0.43	0.025**
Nonpolar aromatic	300 K	0.94 ± 0.45	0.93 ± 0.43	0.86 ± 0.25	0.87 ± 0.35	0.101
	343 K	0.77 ± 0.26	0.68 ± 0.21*	0.74 ± 0.33	0.68 ± 0.21	0.714
	373 K	1.25 ± 0.51	1.05 ± 0.37	1.15 ± 0.45	1.05 ± 0.39	0.094
Polar	300 K	1.03 ± 0.50	1.02 ± 0.46	0.97 ± 0.41	0.92 ± 0.39	0.627
	343 K	0.81 ± 0.35	0.77 ± 0.34*	0.75 ± 0.34	0.74 ± 0.32	0.300
	373 K	1.26 ± 0.58	1.13 ± 0.50	1.31 ± 0.71	1.10 ± 0.48	0.047**
Charged	300 K	1.21 ± 0.58	1.22 ± 0.59	1.22 ± 0.50	1.16 ± 0.50	0.939
	343 K	1.00 ± 0.45	0.97 ± 0.46*	0.97 ± 0.47	1.00 ± 0.50	0.867
	373 K	1.49 ± 0.61	1.40 ± 0.68	1.61 ± 0.93	1.37 ± 0.55	0.101
Negatively charged (Asp, Glu)	300 K	1.08 ± 0.45	1.08 ± 0.40	1.12 ± 0.42	1.05 ± 0.40	0.950
	343 K	0.92 ± 0.35	0.87 ± 0.38*	0.90 ± 0.40	0.90 ± 0.38	0.874
	373 K	1.31 ± 0.47	1.22 ± 0.38	1.35 ± 0.56	1.18 ± 0.42	0.288
Positively charged (Arg, Lys)	300 K	1.45 ± 0.65	1.43 ± 0.74	1.41 ± 0.54	1.39 ± 0.55	0.974
	343 K	1.16 ± 0.52	1.15 ± 0.51*	1.12 ± 0.53	1.20 ± 0.58	0.945
	373 K	1.68 ± 0.69	1.66 ± 0.9	1.94 ± 1.22	1.61 ± 0.59	0.354

*Reference structure
** Significant at α = 0.05

Table 3 — Percentage of compositional differences in the secondary structures at various temperatures and NaCl concentrations in comparison to the reference structure (lipase structure at 343 K and 0.6 M of NaCl).

Temp. (K)	[NaCl] (M)	Compositional difference (%)				
		α-helix	β-sheet	3_{10}-helix	Coil	Turn
300	0	2.43	0.05	-0.44	0.28	-2.32
	0.6	1.93	0.07	-0.28	-0.15	-1.57
	2.0	2.11	0.11	-0.43	-0.19	-1.60
	4.0	1.37	-0.39	-0.80	0.44	-0.62
343	0	3.03	-0.21	-1.47	1.25	-2.60
	0.6	0	0	0	0	0
	2.0	1.57	-0.07	-1.04	0.08	-0.54
	4.0	2.88	0.05	-0.86	0.75	-2.82
373	0	1.53	-0.29	-1.04	0.03	-0.23
	0.6	2.11	-0.01	-0.92	0.17	-1.35
	2.0	1.72	-0.37	-1.07	0.22	-0.50
	4.0	1.94	-0.50	-1.39	-0.03	-0.02

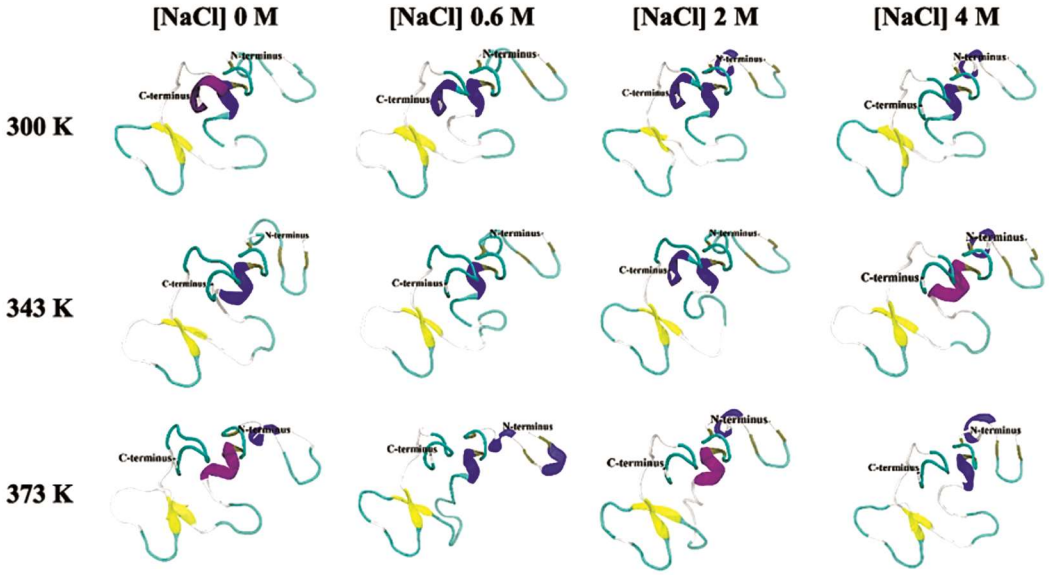


Fig. 3 — The structure of lipase PLS 80 in regions 300-360 at various temperatures and NaCl concentrations. α-helix is shown in purple, β-sheet in yellow, 3_{10}-helix in dark blue, coil in white, and turn in cyan

charged tetrahedral intermediate that forms during the hydrolysis of ester bonds. Stabilisation reduces the activation energy required for the reaction, thereby enhancing the catalytic efficiency of the enzyme[48]. Thus, the fluctuation of the residues in the hole was examined. In the reference structure, Ile, Val, Leu, Leu, His, and Gly residues exhibited RMSF values of 0.62, 0.80, 0.60, 0.67, 1.16, and 0.71 Å, respectively. At 300 K, all residues within the oxyanion hole showed reduced RMSF values compared to those in the reference structure across all simulation conditions, except for Leu9 in the absence of NaCl. At 343 K, the RMSF values for all residues were negative, except for Leu10 at 2 M NaCl. At 373 K, most RMSF values increased, although the H11 and G12 values remained negative. Distance-wise, the RMSF differences of residues in the oxyanion hole were relatively small, ranging from -0.69 to 0.08 Å (Fig. 5).

The changes in hydrogen bonds and electrostatic interactions with Na^+ and Cl^- ions

This study further evaluated whether the relatively small RMSF differences were due to the effects of temperature and NaCl concentration. The evaluation was based on the number of hydrogen bonds and electrostatic interactions of charged residues with Na^+ and Cl^- ions, as both play important roles in

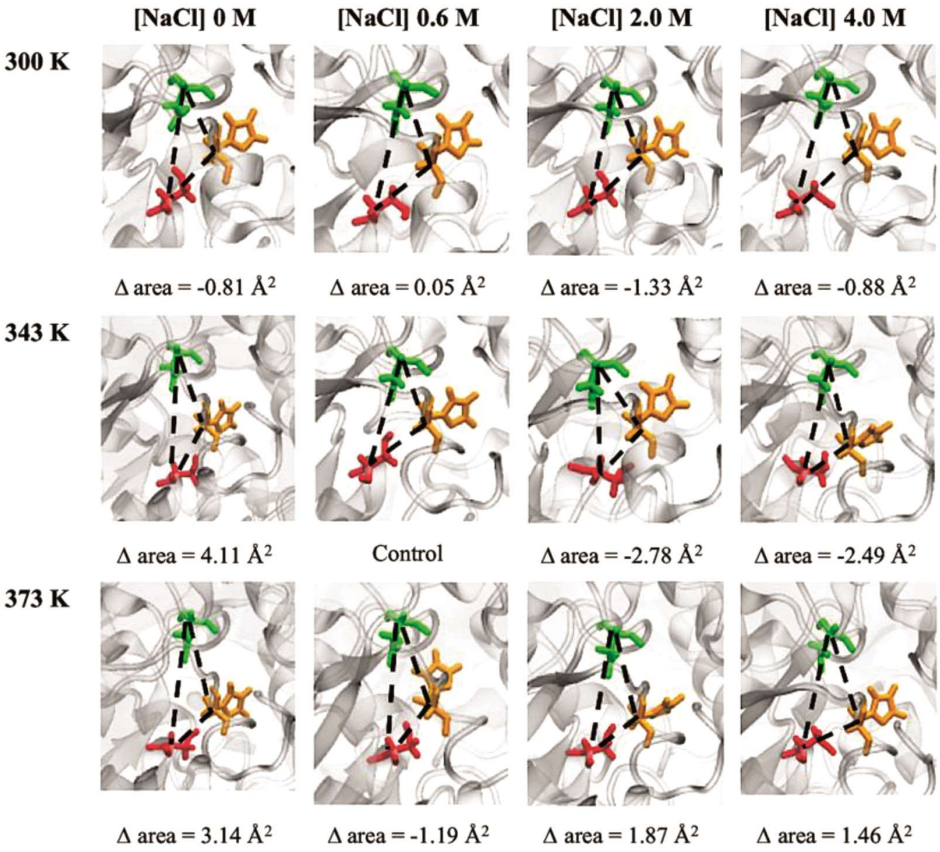


Fig. 4 — Differences in the area and orientation of the catalytic triad at various temperatures and NaCl concentrations. The reference structure was at 343 K and 0.6 M NaCl

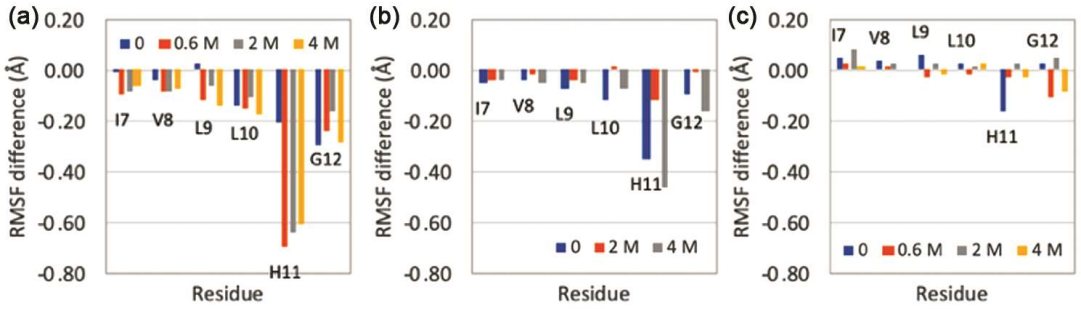


Fig. 5 — Differences in average RMSF values of residues within the oxyanion hole at various temperatures and NaCl concentrations compared to the reference structure (343 K, 0.6 M NaCl). (a) 300 K, (b) 343 K, and (c) 373 K.

thermostability and halostability[44]. Table 4 presents the average number of hydrogen bonds and electrostatic interactions between the charged residues (Glu, Asp, Lys, and Arg) and Na^+/Cl^- ions. The reference structure exhibited 86 hydrogen bonds, 3.7 Glu^-–Na^+, 1.1 Asp^-–Na^+, 2.6 Lys^+–Cl^-, and 5.4 Arg^+–Cl^- interactions.

Generally, the number of hydrogen bonds decreased as the temperature increased and *vice versa*. At 300 K, the number of hydrogen bonds exceeded that of the reference, peaking at 0.6 M NaCl with 96 hydrogen bonds. At 343 K, the number of hydrogen bonds remained consistent across various NaCl concentrations, although it was slightly lower at 4.0 M NaCl. At 373 K, there was a notable reduction in hydrogen bonds, with minimal differences between the different NaCl concentrations (Table 4).

Higher NaCl concentrations significantly enhanced the frequency of electrostatic interactions between charged residues and salt ions. The frequency approximately doubled as the concentration increased

Table 4 — Differences in average hydrogen bonds and electrostatic interactions at various temperatures and NaCl concentrations compared to the reference structure (343 K, 0.6 M NaCl)

Temp.	[NaCl]	Difference in average value				
(K)	(M)	H-bond	Glu^-–Na^+	Asp^-–Na^+	Lys^+–Cl^-	Arg^+–Cl^-
300	0	93	-	-	-	-
	0.6	96	2.7	1.1	2.1	4.1
	2.0	95	6.1	3.1	8.2	14.7
	4.0	91	11.7	6.9	18.4	35.0
343	0	86	-	-	-	-
	0.6	86	3.7	1.1	2.6	5.4
	2.0	86	7.1	3.4	10.5	17.4
	4.0	84	11.8	6.8	22.0	33.3
373	0	79	-	-	-	-
	0.6	80	4.8	1.7	3.3	6.4
	2.0	78	8.1	4.2	11.7	19.9
	4.0	79	11.1	6.2	19.3	34.4

from 0.6 M to 2 M and from 2.0 M to 4.0 M NaCl. A moderate increase in electrostatic interactions was observed with increasing temperature at comparable NaCl concentrations. Notably, the increase in interactions involving positively charged residues was substantially greater than that of negatively charged residues, a trend that was more pronounced at higher ionic strengths. This finding is particularly noteworthy, given the lower number of positively charged residues (12 Lys and 26 Arg) compared to negatively charged residues (22 Asp and 20 Glu) within the structure.

The fluctuations of the positively charged residues (Arg and Lys) were further investigated. The RMFS of Arg in the reference structure (6.8% of the total) ranged from 0.54 to 2.89 Å, whereas that of Lys (3.1% of the total) ranged from 0.75 to 1.79 Å. Arg1 at the terminus was excluded from all calculations because of the fraying. At 300 K, almost all Arg residues showed negative RMSF values regardless of NaCl concentration, with a few exceptions (Fig. 6). At 343 K, the RMSF of Arg residues increased, with notable deviations in Arg 309 and Arg 327. At 373 K, nearly all Arg residues exhibited higher RMSF than the reference, with Arg 309 and Arg 327 at 2 M NaCl displaying the most significant fluctuations. The RMSF differences of Arg across all simulation conditions ranged from -1.09 Å (R150 at 300 K and 2 M NaCl) to 4.96 Å (R327 at 373 K and 2 M NaCl). Similarly, the RMSF patterns for Lys mirrored those of Arg. Lys326 was notably the most fluctuating Lys residue in this structure. The RMSF differences of Lys across all simulation conditions ranged from -0.55 (K248 at 300 K and no NaCl) to 3.76 (K326 at 373 K and 2 M).

Table 5 — The difference in the average total energy at various temperatures and NaCl concentrations. The reference structure was lipase at 343 K and 0.6 M NaCl

Temperature (K)	[NaCl] (M)	The difference in the total energy (kcal/mol)
300	0	-885
	0.6	-726
	2.0	-655
	4.0	-464
343	0	-167
	0.6	0
	2.0	51
	4.0	171
373	0	283
	0.6	565
	2.0	722
	4.0	646

The change in total energy

This study estimated the energy required for lipase to adopt its structure at different temperatures and NaCl concentrations. The total energy was calculated by summing the contributions of the bonds, dihedrals, angular interactions, van der Waals forces, and electrostatic interactions within the protein. The sign and magnitude of the total energy provide insights into conformational stability. The lipase structure at 300 K in the absence of NaCl required 885 kcal/mol less energy than that of the reference. The reference structure had a total energy of -5277 kcal/mol. In general, the energy increased as the NaCl concentration and temperature increased. An exception was observed at 373 K and 4.0 M NaCl, where the energy slightly decreased compared to that at 2.0 M at a similar temperature (Table 5).

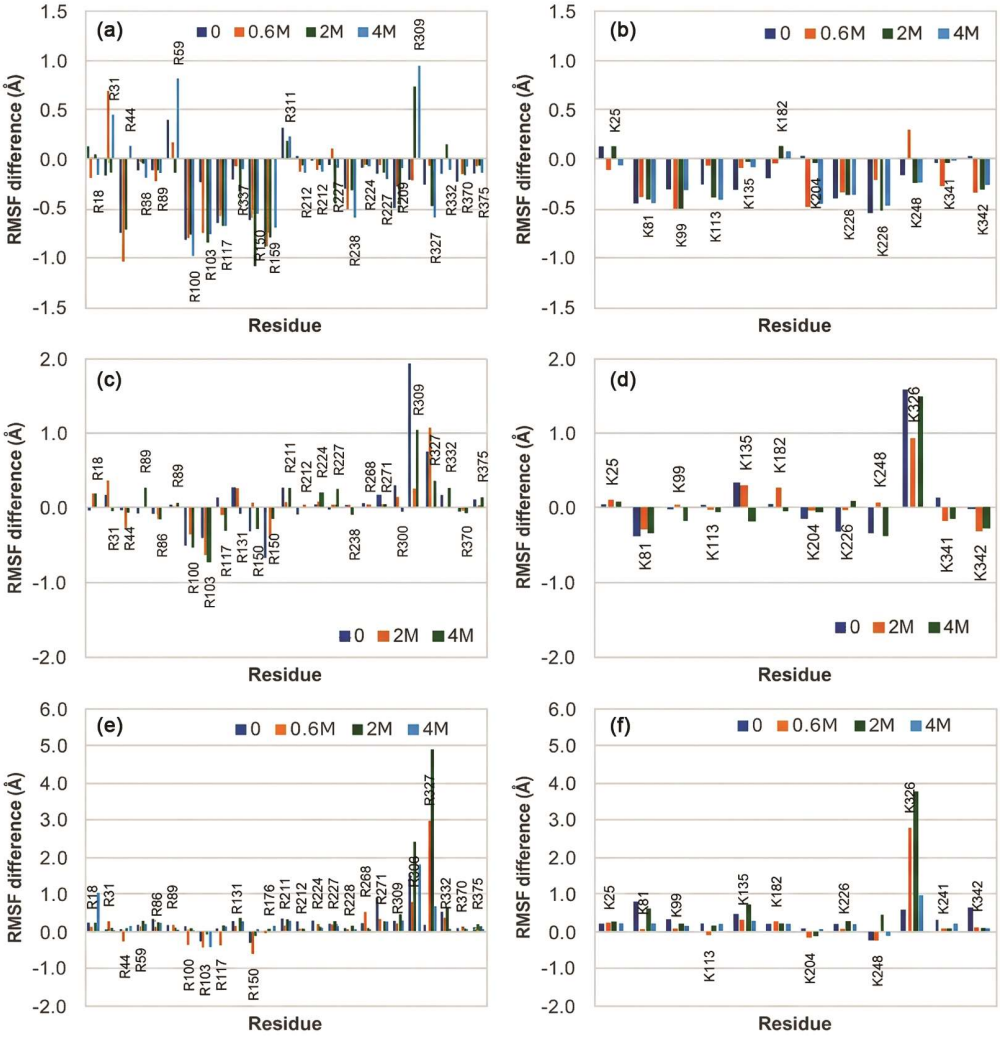


Fig. 6 –Differences in the average RMSF of arginine and lysine at various temperatures and NaCl concentrations compared to the corresponding residues in the reference structure (structure at 343 K and 0.6 M NaCl). (a) Arg at 300 K, (b) Arg at 343 K, (c) Arg at 373 K, (d) Lys at 300 K, (e) Lys at 343 K, and (f) Lys at 373 K. Positive and negative values indicated that the RMSF was higher and lower than that in the reference structure, respectively

Discussion

The computational simulations used in this study were limited by the inherent flexibility of the protein structures, potentially leading to inaccuracies in the observation of certain protein regions[43,49,50]. This study used a simulation system designed to closely replicate native conditions and conducted over extended timescales to facilitate better observations of protein dynamics. However, the limitations of force field algorithms could affect the results[34,51]. Moreover, discrepancies may exist between native and simulated conditions, with unanticipated forces due to the absence of ligands in the structure[52].

Lipase PLS 80 exhibited remarkable stability at various temperatures and NaCl concentrations. When the temperature increased, the structure expanded only slightly. The small changes in the RMSD values indicate that the structural deviation was minimal. The change in R_g was also minimal, with a variation of less than 1%. Regressing the average RMSD against the average R_g values yielded a reasonable positive correlation ($R^2 = 0.881$). In addition, the SASA values varied by approximately 1.3% (Table 1).

The RMSF results support the structural stability assertion. The fluctuation of residues at regions 300-360 was notably higher than that at other regions (Fig. 2). The RMSF values generally increased with increasing temperature but varied unpredictably at different concentrations of NaCl. These results differed from those of a non-thermohalostable protein

(PDB 1BBL), where the structure is greatly affected by increased salt concentrations. It is loose at low salt concentration but more compact at a higher concentration[53].

Based on ANOVA, the effect of NaCl concentration on RMSF was only significant at 373 K but did not affect the charged residues (Table 2). The structural stability claim is also supported by the minor compositional differences in the secondary structure, ranging from -2.82% to 2.88% (Table 3), where the coils and helices contribute more to structural stability[15]. In addition, the differences in RMSF values of residues in the catalytic triad area and oxyanion hole were minor, ranging from -0.35 to -0.39 Å and -0.69 to 0.08 Å, respectively, across all simulation conditions.

Minor differences in the RMSF allow proximal residues to maintain their interactions and catalytic activity. However, the active structural configuration is influenced not only by the distance but also by the bond angles of the interacting residues. For instance, the hydrogen bond distance between the hydroxyl group of Ser and the Nε2 of His in the catalytic triad ranges from 2.0 Å to 2.7 Å, requiring a bond angle between 115° and 140°[54]. Changes in the bond angles can alter the side-chain orientation, thereby affecting the catalytic efficiency. This condition may explain the observed reduction in lipase PLS 80 activity by approximately 10% with a 10°C increase in temperature and a 50% reduction with a 10°C decrease[6], despite the overall structural stability predicted in this simulation. This reduction could be due to the shift in bond orientation of the catalytic triad residues, which were not explored in this study.

The stability of the lipase PLS 80 could be explained by the balance between hydrogen bonds and salt bridges, as well as the presence of salt ions. At elevated temperatures, the number of hydrogen bonds decreased[7]. While the effect of NaCl concentration on the bonds varied at similar temperatures, 0.6 M NaCl was optimal for promoting hydrogen bond formation. In the presence of NaCl, the reduction in hydrogen bonds appears to be compensated for by enhanced electrostatic interactions between charged residues and salt ions[55], although this relationship is not linear. The interactions between Glu^{-}-Na^{+}, Asp^{-}-Na^{+}, Lys^{+}-Cl^{-}, and Arg^{+}-Cl^{-} increased, particularly at higher salt concentrations (Table 4), because more ions were present. Increased NaCl concentrations allow charged surface residues to interact with salt ions, compensating for the loss of hydrogen bonds. The electrostatic equilibrium was maintained by neutralising the amino acid charges, thus preventing aggregation. The stability may also be contributed to by the preservation of key hydrogen bonds near the hydrophobic core to protect against denaturation[56].

In halostable enzymes, salt ions of particular concentration stabilise and compact the structure, thus enhancing its substrate affinity[57]. In this study, moderate salinity counteracts the destabilising effects of elevated temperatures, allowing the molecule to remain flexible yet structurally stable[58,59]. A higher ionic strength screens these interactions and alters the hydration shell, affecting hydrogen bonding with water. It is reported that hydrated electrolyte ions contribute to the solvation shell without excessively competing for water[60]. These factors may explain why lipase exhibited greater stability at 0.6 M NaCl under all simulation conditions.

However, an energy penalty is incurred when the formation of electrostatic interactions with salt ions counteracts the loss of hydrogen bonds. The energy increased as the temperature and salt concentration increased to maintain structural stability (Table 5). This increase can be attributed to several factors. First, electrostatic interactions typically lead to a decrease in entropy compared to hydrogen bonding, as salt ions are more ordered and possess less freedom of movement when bound to molecules[61]. Second, salt ions are usually well hydrated in aqueous solutions, and when they form electrostatic interactions with molecules, they must partially shed their hydration shell, which requires energy[62]. Third, although electrostatic interactions can be strong, hydrogen bonds often provide better geometry and strength for stabilising molecular structures in biological systems[63,64]. Moreover, networks of hydrogen bonds can reinforce each other, providing a cooperative strengthening effect that is often lost when replaced by individual electrostatic interactions[65]. Additionally, hydrogen bonds are generally more specific and directional than electrostatic interactions with salt ions, enhancing the stability of specific conformations[44].

This study suggests that the balance between hydrogen bonds, salt bridges, and interactions with salt ions contributes to enzyme stability under various conditions. However, further investigation into the bond orientations, rotamer preferences and the influence of surrounding residues is required to fully explain the observed changes in the lipase activity.

Conclusion

In conclusion, lipase PLS 80 demonstrated remarkable stability across a range of temperatures and NaCl concentrations with minimal structural deviations. These results suggest that the enzyme maintains its structural integrity primarily through a balance between hydrogen bonds and electrostatic interactions. While increased temperature and salt concentrations disrupt hydrogen bonding networks, the latter may simultaneously enhance electrostatic interactions, thereby supporting the overall stability. However, local structures were affected by the shifting of the secondary structures. The energy costs associated with these interactions are significant, suggesting entropic effects and hydration dynamics during the process. Despite the overall structural stability, the catalytic efficiency may be affected by bond angles; thus, further investigation is necessary to understand this better. These findings highlight the complex interplay between environmental factors and enzyme stability. These findings add to our understanding of lipase stability and its potential applications.

Acknowledgement

This research was supported by Universitas Syiah Kuala through the PTM grant number 449/UN11.2.1/ PT.01.03/PNBP/2023.

Conflict of interest

All authors declare no conflict of interest.

References

1 Burg B van den, Extremophiles as a source for novel enzymes. *Curr Opin Microbiol*, 6 (2003) 213.

2 Capece MC, Clark E, Saleh JK, Halford D, Heinl N, Hoskins S & Rothschild L, Polyextremophiles and the constraints for terrestrial habitability. In: *Cellular origin, life in extreme habitats and astrobiology*, (Ed. by Seckbach J, Oren A & Stan-Lotter H; Springer, Dordrecht) 2013, 7.

3 ur Rehman MF, Shaeer A, Batool AI & Aslam M, Structure-function relationship of extremozymes. In: Microbial extremozymes, (Ed. by Kuddus M; Academic Press, Saudi Arabia) 2022, 9.

4 Elleuche S, Schröder C, Sahm K & Antranikian G, Extremozymes-biocatalysts with unique properties from extremophilic microorganisms. *Curr Opin Biotechnol*, 29 (2014) 116.

5 Kochhar N, Kavya IK, Shrivastava S, Ghosh A, Rawat VS, Sodhi KK & Kumar M, Perspectives on the microorganism of extreme environments and their applications. *Curr Res Microb Sci*, 3 (2022) 100134.

6 Febriani, Aura N, Kemala P, Saidi N & Iqbalsyah TM, Novel thermostable lipase produced by a thermo-halophilic bacterium that catalyses hydrolytic and transesterification reactions. *Heliyon*, 6 (2020) e04520.

7 Iqbalsyah TM, Balqis RC, Febriani & Wahyudi ST, Effect of temperature variation on the structure of gene-translated thermostable lipase by molecular dynamic simulation. *AIP Conf Proc*, 2638 (2022) 040003.

8 Sarmah N, Revathi D, Sheelu G, Yamuna Rani K, Sridhar S, Mehtab V & Sumana C, Recent advances on sources and industrial applications of lipases. *Biotechnol Prog*, 34 (2018) 5.

9 Andreu C, Zarnowski R & del Olmo ML, Recent developments in the biology and biotechnological applications of halotolerant yeasts. *World J Microbiol Biotechnol*, 38 (2022) 27.

10 Yavari-Bafghi M & Amoozegar MA, Pharmaceutical applications of halophilic enzymes. *Heliyon*, 11 (2025) e42754.

11 Pereira JV, Osorio-González CS, Miri S & Brar SK, Petroleum hydrocarbons bioremediation by halotolerant enzymes – Progress & advances. *J Environ Chem Eng*, 12 (2024) 111726.

12 Kumar S, Tsai CJ & Nussinov R, Factors enhancing protein thermostability. *Protein Eng*. 13 (2000) 179.

13 Hung CL, Kuo YH, Lee SW & Chiang YW, Protein stability depends critically on the surface hydrogen-bonding network: A case study of bid protein. *J Phys Chem B*, 125 (2021) 8373.

14 Kumar S, Tsai CJ, Ma B & Nussinov R, Contribution of salt bridges toward protein thermostability. *J Biomol Struct Dyn*, 17 (2000) 79.

15 Ahmed Z, Zulfiqar H, Tang L & Lin H, A statistical analysis of the sequence and structure of thermophilic and non-thermophilic proteins. *Int J Mol Sci*, 23 (2022) 10116.

16 Fukuchi S & Nishikawa K, Protein surface amino acid compositions distinctively differ between thermophilic and mesophilic bacteria. *J Mol Biol*, 309 (2001) 835.

17 Yokota K, Satou K & Ohki S-y, Comparative analysis of protein thermostability: Differences in amino acid content and substitution at the surfaces and in the core regions of thermophilic and mesophilic proteins. *Sci Technol Adv Mater*, 7 (2006) 255.

18 Szilágyi A & Závodszky P, Structural differences between mesophilic, moderately thermophilic and extremely thermophilic protein subunits: Results of a comprehensive survey. *Structure*, 8 (2000) 493.

19 Mitra D & Das Mohapatra PK, Discovery of novel cyclic salt bridge in thermophilic bacterial protease and study of its sequence and structure. *Appl Biochem Biotechnol*, 193 (2021) 1688.

20 Hu G, Luo J, Bao T, Hu X, Yang J & Zhang H, Rational design of disulfide bonds to improve the thermostability and γ-cyclodextrin production capacity of γ-cyclodextrin glycosyltransferase. *Process Biochem*, 144 (2024) 248.

21 Yu K, Chen L, Tang Y, Ma A, Zhu W, Wang H, Tang X, Li Y & Li J, Enhanced thermostability of nattokinase by rational design of disulfide bond. *Microb Cell Fact*, 24 (2025) 51.

22 Scandurra R, Consalvi V, Chiaraluce R, Politi L & Engel PC, Protein thermostability in extremophiles. *Biochimie*, 80 (1998) 933.

23 Madern D, Pfister C & Zaccai G, Mutation at a single acidic amino acid enhances the halophilic behaviour of malate dehydrogenase from Haloarcula marismortui in physiological salts. *Eur J Biochem*, 230 (1995) 1088.

24 Fukuchi S, Yoshimune K, Wakayama M, Moriguchi M & Nishikawa K, Unique amino acid composition of proteins in halophilic bacteria. *J Mol Biol*, 327 (2003) 347.

25 Nayek A, Sen Gupta PS, Banerjee S, Mondal B & Bandyopadhyay AK, Salt-bridge energetics in halophilic proteins. *PLoS One*, 9 (2014) e93862.

26 Lenton S, Walsh DL, Rhys NH, Soper AK & Dougan L, Structural evidence for solvent-stabilisation by aspartic acid as a mechanism for halophilic protein stability in high salt concentrations. *Phys Chem Chem Phys*, 18 (2016) 18054.

27 Wang TN, Guan QT, Pain A, Kaksonen AH & Hong PY, Discovering, characterising, and applying acyl homoserine lactone-quenching enzymes to mitigate microbe-associated problems under saline conditions. *Front Microbiol*, 10 (2019) 823.

28 DasSarma S & DasSarma P, Halophiles and their enzymes: Negativity put to good use. *Curr Opin Microbiol*, 25 (2015) 120.

29 Ebrahimie E, Ebrahimi M, Sarvestani NR & Ebrahimi M, Protein attributes contribute to halo-stability, bioinformatics approach. *Saline System*, 7 (2011) 1.

30 Case DA, Aktulga HM, Belfon K, Ben-Shalom IY, Berryman JT, Brozell SR, Cerutti DS, Cheatham III TE, Cisneros GA, Cruzeiro VWD, Darden TA, Duke RE, Giambasu G, Gilson MK, Gohlke H, Goetz AW, Harris R, Izadi S, Izmailov SA, Kasavajhala K, Kaymak MC, King E, Kovalenko A, Kurtzman T, Lee TS, LeGrand S, Li P, Lin C, Liu J, Luchko T, Luo R, Machado M, Man V, Manathunga M, Merz KM, Miao Y, Mikhailovskii O, Monard G, Nguyen H, O'Hearn KA, Onufriev A, Pan F, Pantano S, Qi R, Rahnamoun A, Roe DR, Roitberg A, Sagui C, Schott-Verdugo S, Shajan A, Shen J, Simmerling CL, Skrynnikov NR, Smith J, Swails J, Walker RC, Wang J, Wang J, Wei H, Wolf RM, Wu X, Y Xiong, Xue Y, York DM, Zhao S & Kollman PA, *Amber 2022 Reference Manual* (University of California, San Francisco) 2022.

31 Arakawa T, Yamaguchi R, Tokunaga H & Tokunaga M, Unique features of halophilic proteins. *Curr Protein Pept Sci*, 18 (2017) 65.

32 Sinha R & Khare SK, Protective role of salt in catalysis and maintaining structure of halophilic proteins against denaturation. *Front Microbiol*, 5 (2014) 165.

33 Case DA, Cheatham TE, Darden T, Gohlke H, Luo R, Merz KM, Onufriev A, Simmerling C, Wang B & Woods RJ, The Amber biomolecular simulation programs. *J Comput Chem*, 26 (2005) 1668.

34 Maier JA, Martinez C, Kasavajhala K, Wickstrom L, Hauser KE & Simmerling C, ff14SB: Improving the accuracy of protein side chain and backbone parameters from ff99SB. *J Chem Theory Comput*, 11 (2015) 3696.

35 Humphrey W, Dalke A & Schulten K, VMD: Visual molecular dynamics. *J Mol Graph*, 14 (1996) 33.

36 Basconi JE & Shirts MR, Effects of temperature control algorithms on transport properties and kinetics in molecular dynamics simulations. *J Chem Theory Comput*, 9 (2013) 2887.

37 Becker OM, MacKerell ADJ, Roux B & Watanabe M, *Computational Biochemistry and Biophysics* (Marcel Dekker Inc, New York) 2001.

38 Coutsias EA, Seok C & Dill KA, Using quaternions to calculate RMSD. *J Comput Chem*, 25 (2004) 1849.

39 Tripathi S, Kumar A, Kahlon AK & Sharma A, Current trends in docking methodologies, In *Oncology: Breakthroughs in research and practice* (IGI Global Scientific Publishing, New York) 2016, 829.

40 Ivankov DN, Bogatyreva NS, Lobanov MY & Galzitskaya OV, Coupling between properties of the protein shape and the rate of protein folding, *PLoS One*, 4 (2009) e6476.

41 Rahban M, Zolghadri S, Salehi N, Ahmad F, Haertlé T, Rezaei-Ghaleh N, Sawyer L & Saboury AA, Thermal stability enhancement: Fundamental concepts of protein engineering strategies to manipulate the flexible structure. *Int J Biol Macromol*, 214 (2022) 642.

42 Ali S, Hassan M, Islam A & Ahmad F, A review of methods available to estimate solvent-accessible surface areas of soluble proteins in the folded and unfolded states. *Curr Protein Pept Sci*, 15 (2014) 456.

43 Narwani TJ, Craveur P, Shinada NK, Santuz H, Rebehmed J, Etchebest C & De Brevern A, Dynamics and deformability of α-, 3_{10}- and π-helices. *Arch Biol Sci*, 70 (2018) 21.

44 Zhou HX & Pang X, Electrostatic interactions in protein structure, folding, binding, and condensation. *Chem Rev*, 118 (2018) 1691.

45 Tanton J, Heron's formula for the area of a triangle, In *Trigonometry a clever study guide* (Mathematical Association of America) 2015, 125.

46 Chen ZS, Wu YD, Hao JH, Liu YJ, He KP, Jiang WH, Xiong MJ, Lv YS, Cao Sl & Zhu J, Molecular dynamic simulation of the porcine pancreatic lipase in non-aqueous organic solvents. *Front Bioeng Biotechnol*, 8 (2020) 676.

47 Miranda R, Lipase gen amplification of thermo-halophilic bacteria isolate Pria Laot Sabang 80 (PLS 80), Undergraduate Thesis, Syiah Kuala University, Banda Aceh, 2019.

48 Mohtashami M, Fooladi J, Haddad-Mashadrizeh A, Housaindokht MR & Monhemi H, Molecular mechanism of enzyme tolerance against organic solvents: Insights from molecular dynamics simulation. *Int J Biol Macromol*, 122 (2019) 914.

49 De Brevern AG, Impact of protein dynamics on secondary structure prediction. *Biochimie*, 179 (2020) 14.

50 Narwani TJ, Craveur P, Shinada NK, Floch A, Santuz H, Vattekatte AM, Srinivan N, Rebehmed J, Gelly JC, Etchebest C & de Brevern AG, Discrete analyses of protein dynamics. *J Biomol Struct Dyn*, 38 (2020) 2988.

51 Petrov D & Zagrovic B, Are current atomistic force fields accurate enough to study proteins in crowded environments? *PLoS Comput Biol*, 10 (2014) e1003638.

52 Fu H, Chen H, Blazhynska M, de Lacam EGC, Szczepaniak F, Pavlova A, Shao X, Gumbart JC, Dehez F, Roux B, Cai W & Chipot C, Accurate determination of protein: Ligand standard binding free energies from molecular dynamics simulations. *Nat Protoc*, 17 (2022) 1114.

53 Shao D, Zhang Q, Xu P & Jiang Z, Effects of the temperature and salt concentration on the structural characteristics of the protein (PDB code 1BBL). *Polymers*, 14 (2022) 2134.

54 Gupta V, Prakash NAU, Lakshmi V, Boopathy R, Jeyakanthan J, Velmurugan D& Sekar K, Recognition of active and inactive catalytic triads: A template based approach. *Int J Biol Macromol*, 46 (2010) 317.

55 Teng R, Zhang J, Tu Z, He Q & Li Y, Computer-aided design to improve the thermal stability of Rhizomucor miehei lipase. *Foods*, 13 (2024) 4023.

56 Benrezkallah D, Molecular dynamics simulations at high temperatures of the Aeropyrum pernix L7Ae thermostable

protein: Insight into the unfolding pathway. *J Mol Graph Model*, 127 (2024) 108700.

57 Zhou S, Pan B, Kuang X, Chen S, Liu L, Song Y, Zhao Y, Xu X, Cheng X & Yang J, Characterisation and mechanism investigation of salt-activated methionine sulfoxide reductase A from halophiles. *iScience*, 27 (2024) 110806.

58 Yang J, Wang Y, Wang L & Zhong D, Mapping hydration dynamics around a β-barrel protein. *J Am Chem Soc*, 139 (2017) 4399.

59 Zhang L, Yang Y, Kao YT, Wang L & Zhong D, Protein hydration dynamics and molecular mechanism of coupled water-protein fluctuations. *J Am Chem Soc*, 131 (2009) 10677.

60 Daronkola HG, Vila Verde A, Proteins maintain hydration at high [KCl] concentration regardless of content in acidic amino acids. *Biophys J*, 120 (2021) 2746.

61 Strickler SS, Gribenko A V., Gribenko A V., Keiffer TR, Tomlinson J, Reihle T, Loladze VV & Makhatadze GI, Protein stability and surface electrostatics: A charged relationship. *Biochemistry*, 45 (2006) 2761.

62 Timasheff SN, Protein hydration, thermodynamic binding, and preferential hydration. *Biochemistry*, 41 (2002) 13473.

63 Kumar S & Nussinov R, Relationship between ion pair geometries and electrostatic strengths in proteins. *Biophys J*, 83 (2002) 1595.

64 van der Lubbe SCC & Guerra CF, The nature of hydrogen bonds: A delineation of the role of different energy components on hydrogen bond strengths and lengths. *Chem - An Asian J*, 14 (2019) 2760.

65 Koch O, Bocola M & Klebe G, Cooperative effects in hydrogen-bonding of protein secondary structure elements: A systematic analysis of crystal data using secbase. *Proteins Struct Funct Genet*, 61 (2005) 310.